Inorg. Chem. **2007**, *46*, 11266–11276

Structural, Thermal, and Magnetic Study of Solvation Processes in Spin-Crossover $[Fe(bpp)_2][Cr(L)(ox)_2]_2 \cdot nH_2O$ Complexes

Miguel Clemente-León,[†] Eugenio Coronado, M. Carmen Giménez-López, and Francisco M. Romero*,[†]

Institut de Ciència Molecular, Universitat de València, Polígon La Coma s/n, E-46980 Paterna, Spain

Received May 10, 2007

The influence of lattice water in the magnetic properties of spin-crossover $[Fe(bpp)_2]X_2 \cdot nH_2O$ salts [bpp = 2,6-bis(pyrazol-3-yl)pyridine] is well-documented. In most cases, it stabilizes the low-spin state compared to the anhydrous compound. In other cases, it is rather the contrary. Unraveling this mystery implies the study of the microscopic changes that accompany the loss of water. This might be difficult from an experimental point of view. Our strategy is to focus on some salts that undergo a nonreversible dehydration–hydration process without loss of crystallinity. By comparison of the structural and magnetic properties of original and rehydrated samples, several rules concerning the role of water at the microscopic level can be deduced. This paper reports on the crystal structure, thermal studies, and magnetic properties of $[Fe(bpp)_2][Cr(bpy)(ox)_2]_2 \cdot 2H_2O$ (**1**), $[Fe(bpp)_2][Cr(phen)(ox)_2]_2 \cdot 0.5H_2O \cdot 0.5MeOH$ (**2**), and $[Fe(bpp)_2][Cr(phen)(ox)_2]_2 \cdot 5.5H_2O \cdot 2.5MeOH$ (**3**). Salt **1** contains both high-spin (HS) and low-spin (LS) Fe^{2+} cations in a 1:1 ratio. Dehydration yields the anhydrous spin-crossover compound with $T_{1/2}\downarrow = 353$ K and $T_{1/2}\uparrow = 369$ K. Rehydration affords the dihydrate $[Fe(bpp)_2][Cr(bpy)(ox)_2]_2 \cdot 2H_2O$ (**1r**) with 100% HS Fe^{2+} sites. Salt **2** also contains both HS and LS Fe^{2+} cations in a 1:1 ratio. Dehydration yields the anhydrous spin-crossover compound with $T_{1/2}\downarrow = 343$ K and $T_{1/2}\uparrow = 348$ K. Rehydration affords $[Fe(bpp)_2][Cr(phen)(ox)_2]_2 \cdot 0.5H_2O$ (**2r**) with 72% Fe^{2+} sites in the LS configuration. The structural, magnetic, and thermal properties of these rehydrated compounds **1r** and **2r** are also discussed. Finally, **1** has been dehydrated and resolvated with MeOH to give $[Fe(bpp)_2][Cr(bpy)(ox)_2]_2 \cdot MeOH$ (**1s**) with 33% HS Fe^{2+} sites. The influence of the guest solvent in the Fe^{2+} spin state can anticipate the future applications of these compounds in solvent sensing.

Introduction

The spin crossover between the low-spin (LS; $S = 0$) and high-spin (HS; $S = 2$) configurations of Fe^{2+} complexes is a well-known example of molecular bistability.[1] The change of the electronic configuration is accompanied by drastic changes in the optical and magnetic properties of these compounds.[2] This can be the basis of optical and/or magnetic commutation effects that can have interesting applications provided that a suitable external stimulus (light irradiation, mechanical perturbation, or thermal change) triggers this process in the solid state at room temperature. The transformation should be abrupt and complete, and this depends on the cooperativity of the system. Thermal hysteresis is observed for strongly cooperative transformations, conferring a memory effect to the system.

Most of the Fe^{2+} complexes undergoing spin crossover have a FeN_6 coordination sphere in octahedral geometry. Among these, an extensive work has been carried out on bischelated complexes of pseudo-C_{2v} symmetry that can be formed using tridentate ligands of the bis(azolyl)pyridine type.[3] In these salts, the imine N atom affords coordination toward Fe^{2+}, whereas the presence of the amino group ensures the formation of strong hydrogen bonds that are very important in defining a peculiarity of these systems: the huge influence of the nature of the counteranions and solvate molecules in the spin-crossover properties.[4] For instance, a systematic study of $[Fe(bpp)_2]X_2 \cdot nH_2O$ salts [bpp = 2,6-bis(pyrazol-3-yl)pyridine; Chart 1] reveals that under ambient

* To whom correspondence should be addressed. E-mail: fmrm@uv.es. Phone: +34 963544405.
[†] Fundació General de la Universitat de València (FGUV).

(1) Gütlich, P.; Goodwin, H. A. *Top. Curr. Chem.* **2004**, *233*, 1.
(2) Gütlich, P.; Hauser, A.; Spiering, H. *Angew. Chem., Int. Ed. Engl.* **1994**, *33*, 2024−2054.
(3) Halcrow, M. A. *Coord. Chem. Rev.* **2005**, *249*, 2880−2908.
(4) Sugiyarto, K. H.; Goodwin, H. A. *Aust. J. Chem.* **1988**, *41*, 1645−1663.

10.1021/ic700910n CCC: $37.00
Published on Web 11/30/2007

Chart 1. Molecular Structure of the Ligand bpp

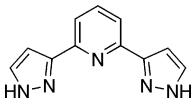

conditions the hydrated species are generally diamagnetic, whereas the corresponding anhydrous compounds are found in the quintet state.[5] Thus, a conversion from the LS state to the HS state is often observed upon dehydration. Interestingly, the anhydrous salts exhibit intrinsic spin crossover at lower temperatures that takes place abruptly and with thermal hysteresis. Anion orientational ordering and $\pi-\pi$ stacking have been proposed in order to account for the strong cooperativity of these anhydrous systems.[6]

At present, attention is paid to the use of spin-crossover compounds for applications like solvent sensing. A wonderful strategy is the obtention of nanoporous materials displaying spin crossover that is influenced by the reversible exchange of solvent molecules.[7−9] The influence of the extent of hydration in the cooperativity and temperature $T_{1/2}$ (where the HS−LS ratio equals to 1) of the spin transition in $[Fe(bpp)_2]^{2+}$ salts makes these compounds also very attractive for practical purposes. In addition, they have the advantage of exhibiting light-induced excited spin state trapping (LIESST) effects at high temperatures with relatively long lifetimes of the photoinduced metastable states.[10,11] However, a thorough determination of the structural and magnetic changes encountered throughout the dehydration−rehydration process has only been performed in a few cases. In a previous Communication, we have reported on the $[Fe(bpp)_2][Cr(bpy)(ox)_2]_2$ system.[12] This salt crystallizes as a dihydrate with two inequivalent (HS and LS) sites, and the corresponding anhydrous compound is a genuine spin-crossover material with $T_{1/2}\uparrow = 369$ K and $T_{1/2}\downarrow = 353$ K. Rehydration takes places irreversibly to a dihydrate showing 100% of HS Fe sites. For the first time, the crystal structure of the rehydrated phase in such a system could be solved. In the present report, we give a detailed account of these sorption−desorption studies and extend our analysis to the related $[Fe(bpp)_2][Cr(phen)(ox)_2]_2$ system (phen = 1,10-phenanthroline).

Experimental Section

$[Fe(bpp)_2][Cr(bpy)(ox)_2]_2\cdot 2H_2O$ (1). A solution containing the ligand bpp [2,6-bis(pyrazol-3-yl)pyridine][13] (140 mg, 0.66 mmol) and $FeSO_4\cdot 7H_2O$ (92 mg, 0.33 mmol) in 40 mL of MeOH was added to a suspension of $Ba[Cr(bpy)(ox)_2]_2\cdot 3H_2O$ (316 mg, 0.33 mmol)[14] in 30 mL of water. After 2 h of stirring, the resulting precipitate was filtered and discarded. Red crystals (199 mg, 53% yield) appeared from evaporation of the filtrate in 3−4 days. IR (KBr, cm^{-1}): 3544 (w), 3444 (w), 3127 (m), 2921 (m), 1711 (vs), 1679 (vs), 1653 (vs), 1609 (s), 1370 (s), 803 (m), 773 (m), 543 (m), 415 (w). Elem. anal. Calcd for $C_{50}H_{38}Cr_2FeN_{14}O_{18}$: C, 46.82; H, 2.99; N, 15.29. Found: C, 46.82; H, 2.93; N, 15.08. Metal anal.: Cr, 65.8; Fe, 34.2.

$[Fe(bpp)_2][Cr(phen)(ox)_2]_2\cdot 0.5H_2O\cdot 0.5MeOH$ (2) and $[Fe(bpp)_2][Cr(phen)(ox)_2]_2\cdot 5.5H_2O\cdot 2.5MeOH$ (3). The procedure is similar to that described above, using $Ba[Cr(phen)(ox)_2]_2\cdot 3H_2O$ (332 mg, 0.33 mmol; phen = 1,10-phenanthroline)[14] instead of the 2,2′-bipyridine (bpy) derivative. After slow evaporation of the filtrate for a couple of days, orange needles of **3** were collected (98 mg, 40% yield). The resulting mother liquor was left standing for 3 weeks to afford red prisms of **2** (31 mg, 15%). Crystals of **2** are very stable toward exposure to ambient atmosphere, whereas crystals of **3** undergo fast desolvation. IR of **2** (KBr, cm^{-1}): 3427 (s), 3126 (w), 3073 (w), 2924 (m), 1709 (vs), 1680 (vs), 1655 (vs), 1576 (s), 1450−1250 (s), 803 (m), 776 (m), 546 (w). Elem. anal. Calcd for **2**: C, 49.60; H, 2.83; N, 14.86. Found: C, 49.34; H, 2.65; N, 14.77. Metal anal. of **2**: Cr, 65.6; Fe, 34.4. IR of **3** (KBr, cm^{-1}): 3427 (s), 3126 (w), 3073 (w), 2924 (m), 1709 (vs), 1680 (vs), 1655 (vs), 1576 (s), 1450−1250 (s), 803 (m), 776 (m), 546 (w). Elem. anal. Calcd for **3**: C, 46.04; H, 3.76; N, 13.30. Found: C, 46.25; H, 3.89; N, 13.87. Metal anal. of **3**: Cr, 64.5; Fe, 35.6.

$[Co(bpp)_2][Cr(bpy)(ox)_2]_2\cdot 2H_2O$ (4). A procedure similar to the synthesis of the Fe analogue (**1**) was employed starting from a solution containing bpp and $CoSO_4\cdot 7H_2O$. IR (KBr, cm^{-1}): 3144 (w), 3117 (w), 3031 (w), 2928 (w), 1711 (vs), 1682 (vs), 1654 (vs), 1609 (s), 1437 (m), 1370 (s), 803 (m), 775 (m), 546 (m). Metal anal.: Cr, 65.8; Co, 34.2.

Physical Techniques. Direct current (dc) magnetic susceptibility measurements were performed on polycrystalline samples using a magnetometer (Quantum Design MPMS-XL-5) equipped with a SQUID sensor. Variable-temperature measurements were carried out in the temperature range 2−400 K in a magnetic field of 0.1 T. The temperature sweeping rate was the same for the experiments performed on the original and methanol-solvated samples, **1** and **1s**: 0.5 K·min^{-1} (2−10 K), 1 K·min^{-1} (10−50 K), 5 K·min^{-1} (50−200 K), and 2 K·min^{-1} (200−400 K). For the rehydrated sample **1r**, the last change in the sweeping rate was set to 340 K. For **2** [and $[Fe(bpp)_2][Cr(phen)(ox)_2]_2\cdot 0.5H_2O$ (**2r**)], instead, the following sequence was used: 0.5 K·min^{-1} (2−20 K) and 2 K·min^{-1} (20−400 K). Finally, the heating rate was decreased for **3** as follows: 0.5 K·min^{-1} (2−20 K) and 1 K·min^{-1} (20−400 K). Dehydrated samples for magnetic measurements were obtained in situ by maintaining the sample in the SQUID at 400 K for 15 min (or until a constant magnetic signal was obtained). All measurements were performed on plastic capsules perforated in order to favor solvent loss. Rehydrated and solvated samples were cooled to 100 K before making the vacuum in the SQUID prechamber.

Thermogravimetric analysis (TGA) measurements were carried out with a Mettler Toledo TGA/SDTA 851 apparatus in the 298−1273 K temperature range under a nitrogen atmosphere and at a scan rate of 5 K·min^{-1}. The dehydration−rehydration processes were monitored by heating grinded samples under a stream of nitrogen from 298 to 383 K (1 K·min^{-1}). Then, the system was kept at this temperature for 20 min to allow complete loss of water molecules. Afterward, the sample was cooled to 298 K. At this

(5) Sugiyarto, K. H.; Craig, D. C.; Rae, A. D.; Goodwin, H. A. *Aust. J. Chem.* **1994**, *47*, 869−890.
(6) Sugiyarto, K. H.; McHale, W. A.; Craig, D. C.; Rae, A. D.; Scudder, M. L.; Goodwin, H. A. *Dalton Trans.* **2003**, 2443−2448.
(7) Halder, G. J.; Kepert, C. J.; Moubaraki, B.; Murray, K. S.; Cashion, J. D. *Science* **2002**, *298*, 1762−1765.
(8) Niel, V.; Thompson, A. L.; Muñoz, M. C.; Galet, A.; Goeta, A. E.; Real, J. A. *Angew. Chem., Int. Ed.* **2003**, *42*, 3760−3763.
(9) Galet, A.; Muñoz, M. C.; Real, J. A. *Chem. Commun.* **2006**, 4321−4323.
(10) Buchen, T.; Gütlich, P.; Sugiyarto, K. H.; Goodwin, H. A. *Chem.−Eur. J.* **1996**, *2*, 1134−1138.
(11) Marcén, S.; Lecren, L.; Capes, L.; Goodwin, H. A.; Létard, J. F. *Chem. Phys. Lett.* **2002**, *358*, 87−95.
(12) Giménez-López, M. C.; Clemente-León, M.; Coronado, E.; Romero, F. M.; Shova, S.; Tuchages, J.-P. *Eur. J. Inorg. Chem.* **2005**, 2783−2787.
(13) Lin, Y.; Lang, S. A. *J. Heterocycl. Chem.* **1977**, *14*, 345−347.
(14) Broomhead, J. A. *Aust. J. Chem.* **1962**, *15*, 228.

Scheme 1

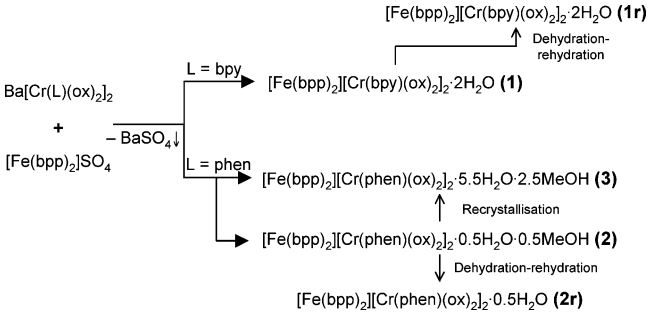

point, the stream of nitrogen was replaced by a stream of humid air to allow complete rehydration of the samples. For the solvation experiment, a stream of nitrogen saturated with dry methanol was used. The total flux of nitrogen was constant during the experiments. After saturation (constant weight), the samples were quickly introduced into the SQUID, protecting them from the environment.

X-ray diffraction measurements were performed on a Nonius Kappa CCD diffractometer equipped with a graphite-monochromated Mo Kα radiation source ($\lambda = 0.7172$ Å). Crystal data were collected at 180 K.[15] The structures were solved by direct methods (*SIR97*)[16] and refined against F^2 with a full-matrix least-squares algorithm using *SHELXL-97*[17] and the *WinGX* (1.64) software package.[18] All non-H atoms were refined anisotropically except for solvent atoms of **3**. H atoms of **2r** and **3** were added in calculated positions and refined riding on the corresponding atoms with the exception of H atoms from water molecules, which were not localized. Instead, H atoms of **2** were located by difference Fourier maps and refined isotropically, with water H atoms being calculated on the basis of geometry and force-field considerations using the *CALC-OH* program.[19] Experimental details concerning X-ray data of **1** and **1r** are given elsewhere.[12]

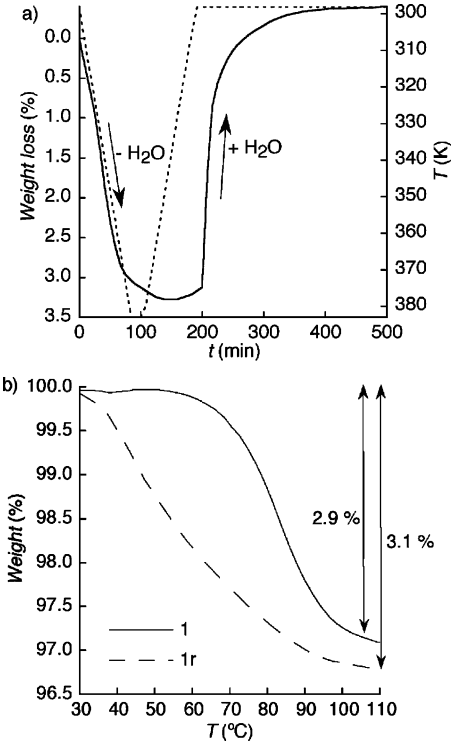

Figure 1. (a) TGA of **1** showing the dehydration−rehydration process. (b) Comparison of the weight loss of original (**1**) and rehydrated (**1r**) samples after thermal treatment in the same conditions.

Heat capacity measurements under a nitrogen atmosphere were performed in a Mettler Toledo DSC 821^e apparatus with warming and cooling rates equal to 4 K·min^{-1}.

IR transmission measurements of KBr pellets were recorded at room temperature with a Nicolet Avatar 320 FT-IR spectrophotometer in the range 4000−400 cm^{-1}.

CHN elemental analyses were carried out in a CE instruments EA 1110 CHNS analyzer. The expected Cr:Fe ratios were confirmed on a Philips ESEM X230 scanning electron microscope equipped with an EDAX DX-4 microsonde.

Results and Discussion

Synthesis and TGA Studies. $[Fe(bpp)_2][Cr(L)(ox)_2]_2$ (L = bpy, phen) systems were obtained by reacting the barium salt $Ba[Cr(L)(ox)_2]_2 \cdot 3H_2O$ with the sulfate salt of the $[Fe(bpp)_2]^{2+}$ complex (Scheme 1). After removal of $BaSO_4$, the bipyridine complex **1** was obtained by slow evaporation of the solvent. In the phen system, two different products were obtained: **2** and **3**. **3** is a less soluble kinetic product obtained after a few hours of evaporation. **2** is a more stable product that crystallizes from the same solution after a few days. It also can be obtained by recrystallization of **3**.

Salts **1** and **2** were submitted to a dehydration−rehydration process to afford the new polymorphs **1r** and **2r**. TGA studies were performed in order to set up the ideal conditions for this experiment. In the following, we will restrict our discussion to the bpy system. The TGA of **1** reveals a 2.9% weight loss between 333 and 383 K (Figure 1a), which can

(15) Crystal data of **2**: $C_{109}H_{70}Cr_4Fe_2N_{28}O_{34}$, $M = 2635.63$, dark-red prism of dimensions 0.40 × 0.40 × 0.04 mm^3, triclinic, $P\bar{1}$, $a = 15.3900(2)$ Å, $b = 17.6000(2)$ Å, $c = 21.5220(3)$ Å, $\alpha = 102.4130(5)°$, $\beta = 101.3390(6)°$, $\gamma = 101.8130(9)°$, $V = 5393.26(12)$ Å^3, $Z = 2$, $\rho_{calcd} = 1.623$ Mg·m^{-3}, μ(Mo Kα) = 0.751 mm^{-1}, $3.20° < 2\theta < 54.96°$. Of 46 741 measured reflections, 24 603 were independent ($R_{int} = 0.0413$) and used to refine 1875 parameters. Final R [$I > 2\sigma(I)$]: R1 = 0.0447, wR2 = 0.1061. Final R (all data): R1 = 0.0829, wR2 = 0.1240. Max and min residual peaks in the final difference map: +0.960 and −1.034 e·Å^{-3}. Crystal data of **2r**: $C_{54}H_{35}Cr_2FeN_{14}O_{16.5}$, $M = 1303.81$, dark-red plate of dimensions 0.30 × 0.3 × 0.03 mm^3, triclinic, $P\bar{1}$, $a = 8.6950(2)$ Å, $b = 15.3770(4)$ Å, $c = 21.4150(6)$ Å, $\alpha = 73.4330(10)°$, $\beta = 78.9940(10)°$, $\gamma = 78.2880(12)°$, $V = 2660.12(12)$ Å^3, $Z = 2$, $\rho_{calcd} = 1.628$ Mg·m^{-3}, μ(Mo Kα) = 0.760 mm^{-1}, $2.00° < 2\theta < 54.36°$. Of 21 273 measured reflections, 11 656 were independent ($R_{int} = 0.1031$) and used to refine 799 parameters. Final R [$I > 2\sigma(I)$]: R1 = 0.0762, wR2 = 0.1912. Final R (all data): R1 = 0.1926, wR2 = 0.2881. Max and min residual peaks in the final difference map: +1.071 and −1.805 e·Å^{-3}. Crystal data of **3**: $C_{56.5}H_{34}Cr_2FeN_{14}O_{24}$, $M = 1452.83$, orange needles of dimensions 0.20 × 0.03 × 0.03 mm^3, monoclinic, $P2_1/a$, $a = 15.5480(5)$ Å, $b = 20.5200(8)$ Å, $c = 21.4760(7)$ Å, $\beta = 98.127(3)°$, $V = 6783.0(4)$ Å^3, $Z = 4$, $\rho_{calcd} = 1.423$ Mg·m^{-3}, μ(Mo Kα) = 0.612 mm^{-1}, $2.76° < 2\theta < 44.40°$. Of 14 726 measured reflections, 8371 were independent ($R_{int} = 0.0667$) and used to refine 874 parameters. The small size of these crystals, together with the presence of microfactures, gave rise to a high mosaicity and to very weak scattering. Because of this, the number of reflections was not enough to carry out anisotropic refinement of all of the atoms. Thus, solvent atoms were refined isotropically. Final R [$I > 2\sigma(I)$]: R1 = 0.0815, wR2 = 0.2410. Final R (all data): R1 = 0.1333, wR2 = 0.2994. Max and min residual peaks in the final difference map: +1.238 and −0.999 e·Å^{-3}.

(16) Altomare, A.; Burla, M. C.; Camalli, M.; Cascarano, G.; Giacovazzo, C.; Guagliardi, A.; Moliterni, A. G. G.; Polidori, G.; Spagna, R. *J. Appl. Crystallogr.* **1999**, *32*, 115.

(17) Sheldrick, G. M. *SHELXL-97. Program for the refinement of crystal structures from diffraction data*; University of Göttingen: Göttingen, Germany, 1997.

(18) Farrugia, L. J. *J. Appl. Crystallogr.* **1999**, *32*, 837.

(19) Nardelli, M. *J. Appl. Crystallogr.* **1999**, *32*, 563.

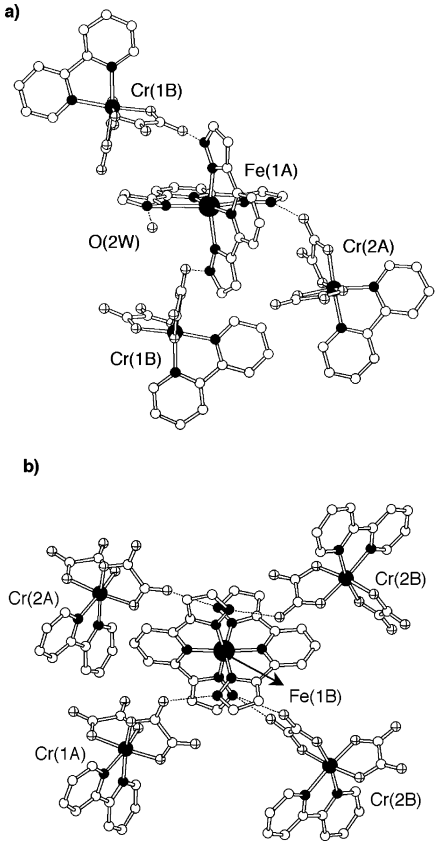

Figure 2. Plots of the crystal structure of **1** showing the first and second coordination spheres of the two nonequivalent (a) HS [Fe(1A)] and (b) LS [Fe(1B)] cations.

be attributed to the loss of two water molecules per formula unit. The dihydrate formulation is in agreement with the elemental analysis and the X-ray crystal structure determination (see below). When the anhydrous compound is exposed to the open air, the two water molecules are recovered in a few hours. The sample can be submitted to several consecutive dehydration−rehydration experiments with no apparent degradation. It seems, however, that the water molecules in the rehydrated phase (**1r**) are less tightly bound to the crystal lattice than those in **1** (Figure 1b).

Structural Study of the $[Fe(bpp)_2][Cr(bpy)(ox)_2]_2$ System. 1 crystallizes in the triclinic system ($P\bar{1}$ space group). Its structure comprises isolated $[Fe(bpp)_2]^{2+}$ and $[Cr(bpy)(ox)_2]^-$ complex ions together with water molecules. Two inequivalent Fe^{2+} sites, named Fe(1A) and Fe(1B), were found (Figure 2). Both centers adopt a slightly distorted C_{2v} symmetry, with the tridentate bpp ligand binding to the metal ion in meridional positions. The Fe(1A)−N distances lie in the range 2.146(2)−2.210(2) Å and are characteristic of the HS configuration. In contrast, Fe(1B)−N distances are shorter [1.921(2)−1.976(2) Å) and typical of LS Fe^{2+}. Thus, the structure determination shows the coexistence of HS and LS Fe^{2+} centers in the same crystalline phase. This situation has been found previously and can be attributed to marked differences in their second coordination spheres.[20] In our case, the four noncoordinating −NH groups of complex **A** are

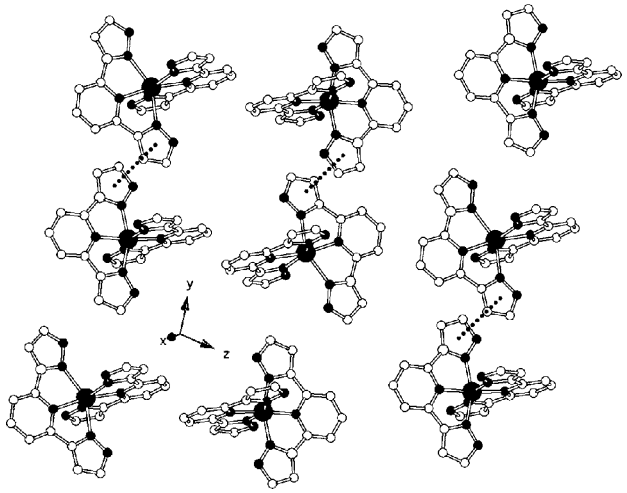

Figure 3. View of the crystal structure of **1** showing the arrangement of $[Fe(bpp)_2]^{2+}$ units. The dashed lines refer to $\pi-\pi$-stacking interactions.

hydrogen-bonded to three $[Cr(bpy)(ox)_2]^-$ anions and one water molecule O(2W), whereas complex **B** is surrounded by four $[Cr(bpy)(ox)_2]^-$ anions at hydrogen-bonding distances. Because the terminal O atom of oxalate in $[Cr(bpy)(ox)_2]^-$ is a better hydrogen-bonding acceptor than water, the electron density in the corresponding pyrazolyl ring of **B** is increased with respect to **A**, leading to a strengthening of the N(imine)−Fe(1B) σ bond. This favors the LS state for the Fe(1B) center.

The crystal structure exhibits four crystallographically independent Cr^{3+} sites [Cr(1A), Cr(1B), Cr(2A), and Cr(2B)]. The Cr^{3+} ions adopt a slightly distorted N_2O_4 octahedral geometry with one bpy ligand and two oxalate anions binding in a chelate mode. The distortion is primarily due to the different bite angles of bipyridine [78.72(10)−79.27(9)°] and oxalate [81.84(9)−83.46(8)°] chelates. The Cr−O(ox) bond distances [1.937(2)−1.966(2) Å] are shorter than those of Cr−N(bpy) [2.048(3)−2.063(2) Å], as was already observed in previously reported $[Cr(L)(ox)_2]^-$ salts.[21] The two bpy ligands coordinated to Cr(1A) and Cr(2A) deviate strongly from a coplanar configuration. The tilt angles between their pyridine rings [17.12(7)° and 14.57(7)°, respectively] are much higher than those observed for Cr(1B) and Cr(2B) [6.55(7)° and 6.48(7)°, respectively].

In the search of the origin of cooperativity, the crystal packing was also analyzed with special attention to the aryl−aryl interactions between bpp ligands. The packing is formed by alternating layers of $[Fe(bpp)_2]^{2+}$ cations and $[Cr(bpy)(ox)_2]^-$ anions. In the cationic layers, $[Fe(bpp)_2]^{2+}$ units are organized into dimers by $\pi-\pi$-stacking interactions (Figure 3). The distance between the bpp mean planes within the dimer is 3.204(3) Å. In the anionic layers, aryl−aryl interactions between bpy ligands belonging to adjacent Cr^{3+} complexes are also observed, with values for the interplanar distance in the range 3.583(2)−3.742(1) Å. These contacts organize anions in stacks running parallel to the *b* axis (see the Supporting Information). Similar stacking motifs have been

(20) Sugiyarto, K. H.; Scudder, M. L.; Craig, D. C.; Goodwin, H. A. *Aust. J. Chem.* **2000**, *53*, 755−765.

(21) Rochon, F. D.; Melanson, R.; Andruh, M. *Inorg. Chem.* **1996**, *35*, 6086−6092.

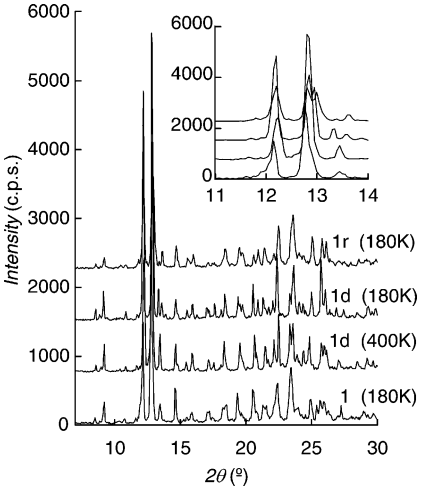

Figure 4. Powder X-ray diffractograms of original (**1**), dehydrated (**1d**), and rehydrated (**1r**) compounds. The inset shows an enlargement of the low-angle region. The temperature of the measurement is quoted in parentheses.

found in previously reported $[Cr(L)(ox)_2]^-$ salts.[22] Finally, cationic and anionic layers are interconnected by an intricate hydrogen-bonded network involving water molecules.

The structural changes that take place upon dehydration and subsequent rehydration of **1** were followed by powder X-ray diffraction (Figure 4). The X-ray diffractogram of the original sample at 180 K matches the simulated data obtained from the single-crystal analysis. After dehydration at 400 K, the X-ray pattern changes slightly: some peaks at higher angles are doubled, and the most intense peaks shift to higher 2θ values. Interestingly, the diffractogram of the dehydrated sample at 400 K differs from that obtained at 180 K, giving a first indication of a phase transition in the $180 < T < 400$ K temperature range. When the sample is submitted to rehydration, the observed structural pattern differs only slightly from that observed for the dehydrated and original samples. Clearly, the crystallinity of the sample is not altered by the dehydration−rehydration process. This prompted us to determine the crystal structure of the rehydrated compound (**1r**) by a single-crystal X-ray analysis.

1r is also a dihydrate and crystallizes in the $P\bar{1}$ space group. The volume of the unit cell is now halved compared to **1**. There is only one independent Fe^{2+} center and two inequivalent Cr^{3+} complexes. The Fe−N distances are characteristic of HS Fe^{2+} and lie in the 2.145(3)−2.204(3) Å range. Bond distances and bond angles in the iron coordination sphere are similar to those observed for the HS Fe(1A) center of **1**. The second coordination sphere is also similar: the amino groups of bpp ligands are connected to one water molecule, O(2W), and three $[Cr(bpy)(ox)_2]^-$ anions through hydrogen bonding (Figure 5). This confirms that the presence of the water molecule (a poorer hydrogen-bond acceptor) in the vicinity of the Fe^{2+} complex stabilizes a HS configuration.

The structure of **1r** can also be viewed as an alternating arrangement of cationic $[Fe(bpp)_2]^{2+}$ and anionic $[Cr(L)(ox)_2]^-$

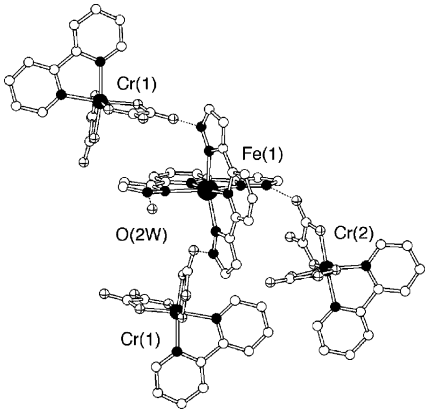

Figure 5. Plot of the crystal structure of **1r** showing the first and second coordination spheres of the HS Fe^{2+} cation.

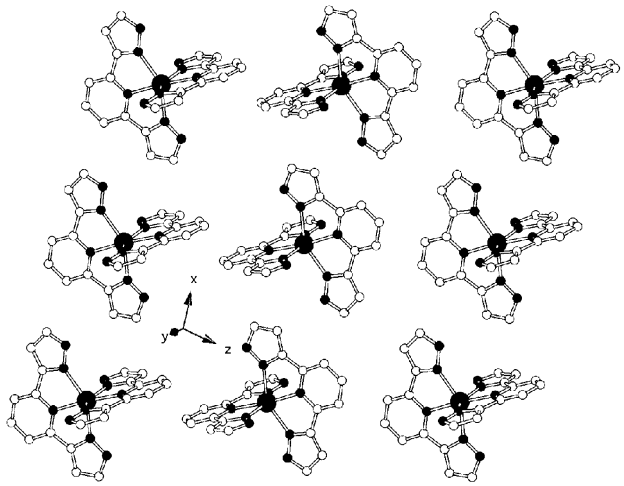

Figure 6. View of the crystal structure of **1r** showing the arrangement of $[Fe(bpp)_2]^{2+}$ units.

layers connected via hydrogen bonds. The stacking motifs are maintained within the chromium layers. However, the number of hydrogen bridges is considerably decreased, and the water molecules are less tightly bonded to the complex ions. Another difference is that the aryl−aryl interactions between Fe^{2+} complexes are not observed (Figure 6). All of these aspects might affect the equilibrium between the HS and LS states, although it seems that the relative strength of hydrogen bonding to the counterion/solvate is the important factor in defining the spin state for the spin-crossover units.

Structural Study of the $[Fe(bpp)_2][Cr(phen)(ox)_2]_2$ System. 2 crystallizes in the same space group ($P\bar{1}$) as **1** with similar values of the cell parameters. The main difference between the two structures concerns the presence of solvent molecules: **1** is a dihydrate, whereas in **2** the isolated $[Fe(bpp)_2]^{2+}$ and $[Cr(phen)(ox)_2]^-$ complex ions sit together with $0.5H_2O$ and 0.5MeOH molecules per formula unit. As in **1**, two inequivalent Fe^{2+} sites [Fe(1A) and Fe(1B)] and four inequivalent chromium sites [Cr(1A), Cr(1B), Cr(2A) and Cr(2B)] were found (Figure 7). The coordination spheres of Fe(1A) and Fe(1B) are very similar to those found in **1**. The Fe(1A)−N distances [2.159(2)−2.229(2) Å] agree with a HS configuration, whereas the Fe(1B)−N distances [1.924(2)−1.985(2) Å] are typical of LS Fe^{2+}. Again, in the HS complex **A**, the four noncoordinating −NH groups are

(22) Muñoz, M. C.; Julve, M.; Lloret, F.; Faus, J.; Andruh, M. *J. Chem. Soc., Dalton Trans.* **1998**, 3125.

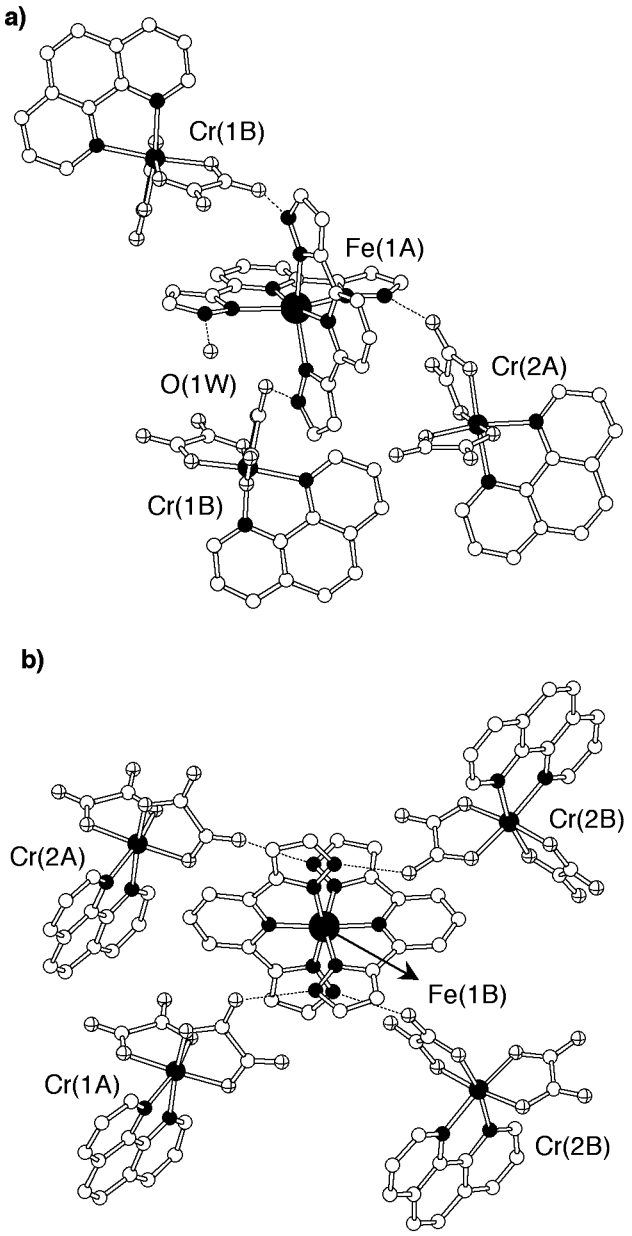

Figure 7. Plots of the crystal structure of **2** showing the first and second coordination spheres of the two nonequivalent (a) HS [Fe(1A)] and (b) LS [Fe(1B)] cations.

hydrogen-bonded to three $[Cr(phen)(ox)_2]^-$ anions and one water molecule, O(1W), whereas the LS complex **B** is surrounded by four $[Cr(phen)(ox)_2]^-$ anions. This is a further confirmation of the role played by the water molecule in destabilizing the LS state. The Cr^{3+} sites adopt a geometry similar to that of **1**. The only remark concerns the tilt angles between the pyridine rings that are smaller due to the rigidity of the phen ligand.

The crystal packing is also very similar to that previously described for **1** and can be viewed as formed by alternating layers of $[Fe(bpp)_2]^{2+}$ cations and $[Cr(phen)(ox)_2]^-$ anions (see the Supporting Information). The presence of $\pi-\pi$ stacking interactions between the pyrazolyl units organize dimers separated by a distance lying in the range 3.273(2)−3.490(4) Å. The typical 1D stacking motif encountered in other $[Cr(L)(ox)_2]^-$ salts is also observed here. It is built from

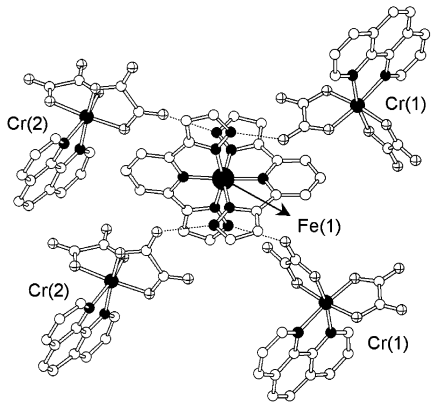

Figure 8. Plot of the crystal structure of **2r** showing the first and second coordination spheres of the Fe^{2+} cation.

aryl−aryl interactions [interplanar distance in the range 3.545(2)−3.724(3) Å] between phen ligands belonging to adjacent Cr^{3+} complexes. The water molecule connects one $[Fe(bpp)_2]^{2+}$ unit to two chromate anions, whereas the methanol molecule is only connected to one $[Cr(phen)(ox)_2]^-$ complex.

Crystals of **2** were also submitted to a desolvation−rehydration process, and the crystallinity of the sample was maintained. We could then analyze the structure of the rehydrated compound **2r** in comparison with the original salt **2**. Both solvates crystallize in the $P\bar{1}$ space group. The cell volume of the rehydrated compound is again halved compared to the original one. Only one independent Fe^{2+} center and two inequivalent Cr^{3+} complexes are found. The Fe−N distances span over a wide range [1.914(6)−2.013(7) Å] but point clearly to the presence of LS Fe^{2+}. This is in contrast with the bpy-based system, where rehydration stabilizes the HS state. The explanation is again given by examination of the Fe^{2+} surroundings: in **2r**, the amino groups of the Fe^{2+} complex bind to four $[Cr(phen)(ox)_2]^-$ anions (Figure 8). The water molecule is not present in the second coordination sphere, being loosely connected to an oxalate anion of a Cr^{3+} unit. Again, a second coordination sphere formed by four anions seems to favor the LS state. However, the examination of the crystal packing reveals strong bpp−bpp stacking interactions that organize chains running along the *a* axis (Figure 9). This is in contrast with the HS rehydrated compound **1r**, where no significant interactions between Fe^{2+} complexes were observed. Clearly, both hydrogen-bonding and aryl−aryl interactions can be correlated with the Fe^{2+} spin state.

The crystal structure of **3** was also solved by single-crystal X-ray diffraction. **3** crystallizes in the monoclinic $P2_1/a$ space group. Only one Fe^{2+} and two Cr^{3+} sites were found in the asymmetric unit. The Fe^{2+} coordination sphere differs from those of the previous compounds in that the dihedral angle between bpp ligands [82.56(10)°] deviates considerably from 90°. Fe−N bond distances lie in the range 2.145(7)−2.212(7) Å and are characteristic of a HS configuration. Strikingly, the second coordination sphere is formed by four $[Cr(phen)(ox)_2]^-$ anions at hydrogen-bonding distances from the pyrazolyl N−H groups (Figure 10). This result was unexpected in view of the precedent compounds that showed invariably a LS

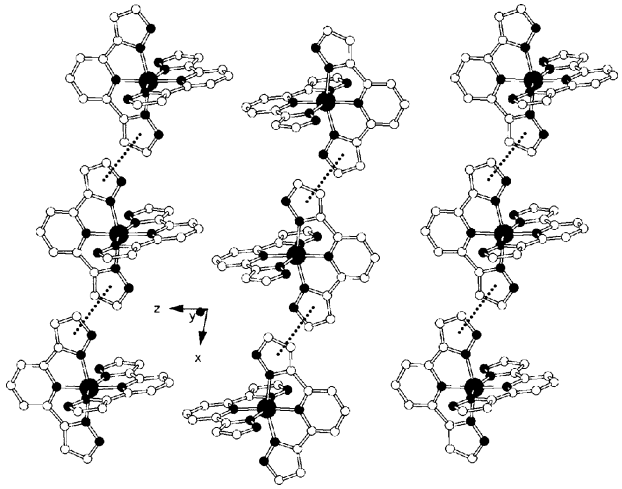

Figure 9. View of the crystal structure of **2r** showing the arrangement of $[Fe(bpp)_2]^{2+}$ units. The dashed lines refer to $\pi-\pi$-stacking interactions.

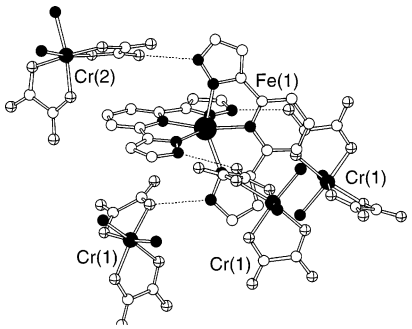

Figure 10. Plot of the crystal structure of **3** showing the first and second coordination spheres of the Fe^{2+} cation. The ligand phen C atoms have been omitted for the sake of clarity.

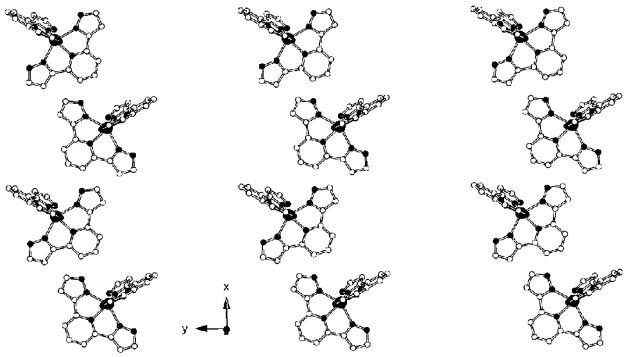

Figure 11. View of the crystal structure of **3** showing the arrangement of $[Fe(bpp)_2]^{2+}$ units.

state for the Fe^{2+} complexes in similar surroundings. The difference in behavior might be attributed to the fact that one of the N−H groups is connected to a Cr(1)-bonded O atom. This situation might favor the HS state because metal-bonded O atoms are poorer hydrogen-bond acceptors than terminal ones.

Another possible explanation can be given by examining the packing of $[Fe(bpp)_2]^{2+}$ cations, which is very different from the previous examples (Figure 11). In the present case, the Fe^{2+} complexes are well-isolated in the *y* direction due to the presence of stacks of anions. In the *x* direction, the relative orientation of adjacent molecules excludes any

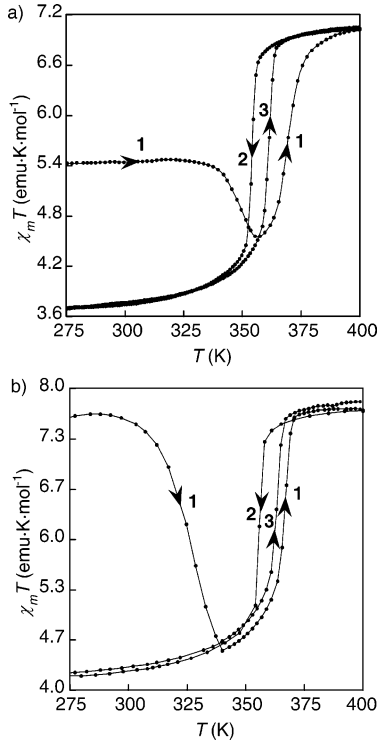

Figure 12. Temperature dependence of χT for **1** (a) and **1r** (b). Curve 1: first heating. Curves 2 and 3: subsequent temperature cycles (cooling and heating, respectively).

possibility of stacking interactions. It seems that the absence of aryl−aryl interactions favors a HS configuration for the Fe^{2+} sites.

Magnetic Properties of the $[Fe(bpp)_2][Cr(bpy)(ox)_2]_2$ System. Figure 12a shows the thermal variation (heating mode, curve 1) of the χT product (χ = molar magnetic susceptibility; T = absolute temperature) of **1**. From low temperature to 320 K, a roughly constant χT product equal to 5.5 emu·K·mol^{-1} is observed. This value is in agreement with the presence of 50% of the Fe^{2+} cations in the HS state, as was already deduced from X-ray diffraction. It is somewhat higher than the "spin-only" value (χT = 5.25 emu·K·mol^{-1}) calculated for two Cr^{3+} ions and $^1/_2$ Fe^{2+} per formula unit, as expected from the existence of orbital contributions. Upon heating above 320 K, χT decreases to reach a minimum at 365 K, and then it increases to reach a constant value of 7 emu·K·mol^{-1} at 400 K. This is again slightly higher than the expected "spin-only" value for one Fe^{2+} and two Cr^{3+} ions per formula (χT = 6.75 emu·K·mol^{-1}), indicating that 100% of the iron sites are in the HS configuration. Upon cooling now the sample (curve 2) below 300 K, a constant χT value of 3.7 emu·K·mol^{-1} is obtained, which is close to the one expected for two uncorrelated Cr^{3+} ions with 100% of Fe^{2+} in the LS state. Thus, the anhydrous salt $[Fe(bpp)_2][Cr(bpy)(ox)_2]_2$ undergoes a spin transition with $T_{1/2}\downarrow$ = 353 K. Finally, curve 3 reveals a hysteretic behavior given by $\Delta T = T_{1/2}\uparrow - T_{1/2}\downarrow$ = 16 K.

The initial decrease of χT for the original sample between 320 and 365 K is sweep-rate-dependent, and TGA measurements (vide supra) show the loss of water molecules in this temperature range. Clearly, Fe(1A) atoms are changing their

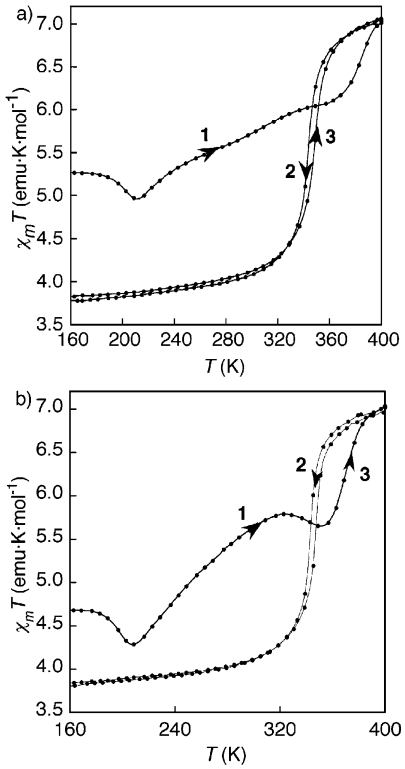

Figure 13. Temperature dependence of χT for **2** (a) and **2r** (b). Curve 1: first heating. Curves 2 and 3: subsequent temperature cycles (cooling and heating, respectively).

configuration from the HS state to the LS state during dehydration. This is in contrast with all previously reported $[Fe(bpp)_2]X_2 \cdot nH_2O$ salts, where dehydration forces the reversed transformation (LS → HS).[5] The difference is due to the fact that the spin transition of the anhydrous salt is now pushed to higher temperatures: when dehydration starts, the anhydrous compound is still in the LS state.[23]

The rehydrated material **1r** shows a completely different magnetic behavior. Below room temperature (Figure 12b, curve 1), χT is nearly constant and equal to 7.5 emu·K·mol^{-1}, indicating that 100% of the Fe^{2+} sites are HS. Above 300 K, χT decreases to reach a minimum at 340 K and then increases abruptly to a value of 7.5 emu·K·mol^{-1}. Successive temperature cycles (curves 2 and 3) reveal that the abrupt increase corresponds to the intrinsic spin transition of the dehydrated compound. Again, the minimum depends very strongly on the sweeping rate, and its presence is due to dehydration of the sample stabilizing the LS state. The temperature of the minimum (340 K) is lower than that found in **1** (365 K) in the same conditions. This means that water molecules are now less tightly bound in the crystal lattice, as suggested by the TGA measurements.

Magnetic Properties of the $[Fe(bpp)_2][Cr(phen)(ox)_2]_2$ System. Figure 13a shows the temperature dependence (heating mode, curve 1) of χT for **2**. From low temperature to 180 K, χT remains constant and equal to 5.27 emu·K·mol^{-1}. As was already discussed for **1**, this value is in agreement with the presence of 50% of the Fe^{2+} cations in the HS state

(23) Sugiyarto, K. H.; Craig, D. C.; Rae, A. D.; Goodwin, H. A. *Aust. J. Chem.* **1993**, *46*, 1269−1290.

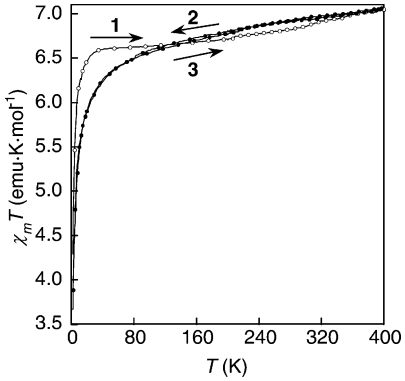

Figure 14. Temperature dependence of χT for **3**. Curve 1: first heating. Curves 2 and 3: subsequent temperature cycles (cooling and heating, respectively).

and confirms the structural data. Upon heating above 180 K, a slight decrease of χT to a minimum value of 4.9 emu·K·mol^{-1} at 212 K is observed. Further heating yields a gradual increase of χT that becomes more abrupt at temperatures higher than 370 K. At 400 K, χT equals 7 emu·K·mol^{-1}, indicating that 100% of the iron sites are in the HS configuration. The dehydrated compound $[Fe(bpp)_2][Cr(phen)(ox)_2]_2$ obtained at this temperature undergoes also complete spin transition (curves 2 and 3) with parameters $T_{1/2}\downarrow = 343$ K and $T_{1/2}\uparrow = 348$ K. Compared to the bpy system, the transition takes place at lower temperatures and it is less cooperative. The more bulky phen ligands might separate the Fe^{2+} sites at a higher distance compared with bpy.

The thermal variation of χT for the rehydrated phase **2r** is shown in Figure 13b. From low temperature to 180 K (heating mode, curve 1), χT exhibits a plateau at 4.7 emu·K·mol^{-1}. This value indicates a HS content of 28%. This is in contradiction with the structural data, which point to a LS configuration for the Fe^{2+} cation. Upon heating above 180 K, a slight decrease of χT to a minimum value of 4.3 emu·K·mol^{-1} at 208 K is observed. Further heating yields a gradual increase of χT to reach a maximum at 320 K. In the 320−350 K range, χT decreases smoothly on increasing the temperature, and then it increases abruptly to reach a value of 7 emu·K·mol^{-1} at 400 K, where 100% of the iron sites are in the HS configuration. As expected, the dehydrated compound $[Fe(bpp)_2][Cr(phen)(ox)_2]_2$ undergoes complete spin transition (curves 2 and 3) with parameters $T_{1/2}\downarrow = 343$ K and $T_{1/2}\uparrow = 348$ K.

The χT vs T plot for **3** (Figure 14, curve 1) exhibits a plateau in the 40−250 K range with a value of 6.6 emu·K·mol^{-1}. Upon further heating to the maximum temperature of the experiment (400 K), a slight and gradual increase to 7 emu·K·mol^{-1} is observed. It appears that at room temperature most of the Fe^{2+} sites are HS, in agreement with the X-ray data. However, a residual fraction (around 10%) of LS centers is also present in the material. This fraction undergoes spin change (LS → HS) subsequent to desolvation. Upon cooling (curves 2 and 3), a smooth and reversible decrease of χT is detected. It seems that only a small portion of the Fe^{2+} cations change their spin in a gradual way. This is striking when compared to the dehy-

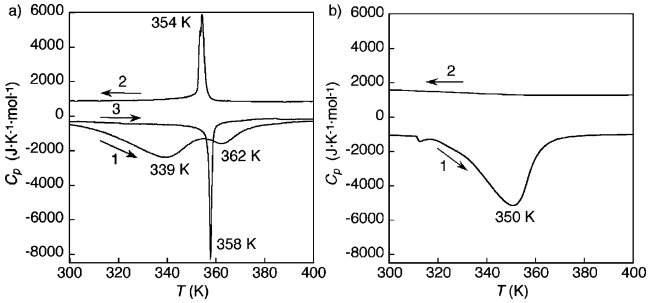

Figure 15. DSC of **1** (a) and **4** (b). Curve 1: first heating. Curves 2 and 3: subsequent temperature cycles (cooling and heating, respectively).

drated material obtained from **2**, which exhibits an abrupt phase transition. It seems that the two solvates **2** and **3** afford different crystal phases of the dehydrated material. This is not strange in view of the different symmetries of their crystal packings.

Calorimetric Studies of the $[Fe(bpp)_2][Cr(bpy)(ox)_2]_2$ System. Differential scanning calorimetry (DSC) measurements were performed in order to have an additional proof of the nature of the different phase transitions suggested by the magnetic studies. For **1**, the specific heat measurement in the first heating process (Figure 15a, curve 1) exhibits two large endothermic peaks. The first peak centered at 339 K corresponds to the loss of water molecules, and the second peak centered at 362 K is mostly associated with the initial LS → HS conversion. Upon cooling to room temperature (curve 2), two very close exothermic peaks around 354 K are observed. They are assigned to the abrupt spin transition (HS → LS) already shown in the magnetic measurements. The second heating experiment (curve 3) reveals now a single sharper peak (annealing) at 358 K. The thermal hysteresis of the anhydrous material is much smaller than that observed in the magnetic measurements, probably due to the different conditions of dehydration, heating rates, etc. It is interesting to compare the DSC data of **1** with those recorded for the isostructural Co^{2+} analogue **4**. The Co^{2+} compound (Figure 15b) shows also a very large endothermic peak centered at 350 K corresponding to loss of water. In the cooling mode, however, a featureless curve is obtained. This fact could be anticipated because **4** is a HS Co^{2+} complex in the whole temperature range (see the Supporting Information). This unambiguously confirms the assignment made for **1**: dehydration takes place with a subsequent spin change during the first heating.

The rehydrated compound **1r** exhibits a different behavior (Figure 16). In the first heating process (curve 1), dehydration takes place at lower temperatures (323 K) compared to **1**. The two endothermic peaks are well-separated, and the spin transition is seen as a sharper peak. Finally, curves 2 and 3 give the characteristic spin-crossover response of the dehydrated material. The thermal hysteresis obtained from DSC measurements is 6 K.

Calorimetric Studies of the $[Fe(bpp)_2][Cr(phen)(ox)_2]_2$ System. The thermal properties of the two solvates **2** and **3** were also analyzed by DSC. For **2**, the first heating process (Figure 17a, curve 1) reveals a single and very large endothermic peak centered at 388 K. This temperature

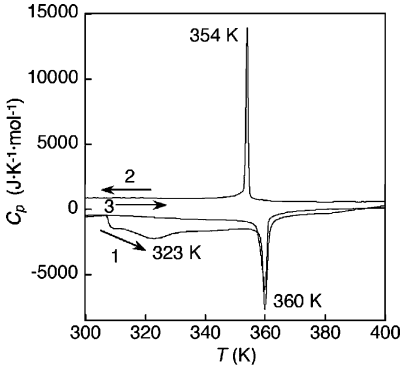

Figure 16. DSC of **1r**. Curve 1: first heating. Curves 2 and 3: subsequent temperature cycles (cooling and heating, respectively).

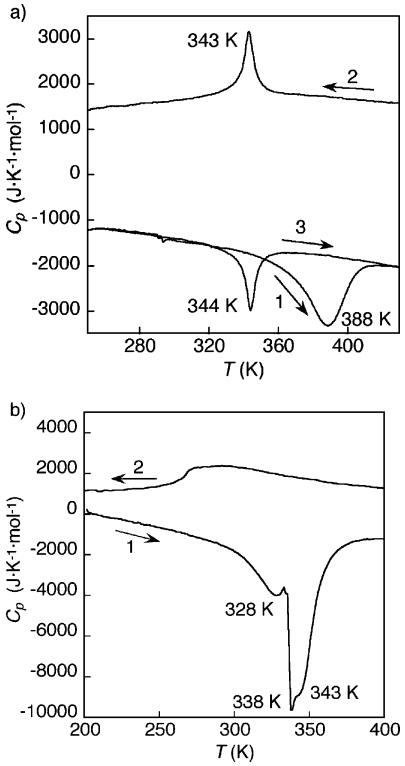

Figure 17. DSC of **2** (a) and **3** (b). Curve 1: first heating. Curves 2 and 3: subsequent temperature cycles (cooling and heating, respectively).

corresponds to the point of maximum slope in the $\chi T = f(T)$ curve. Clearly, in this case, the loss of water takes place at higher temperatures, being concomitant with the LS → HS spin transition. In the cooling process (curve 2), an exothermic peak at 343 K is observed. This peak is larger compared to that measured for the bpy derivative **1**, indicating that the spin transition is less cooperative and occurs at lower temperatures. The second heating experiment (curve 3) yields a single peak at 344 K. The small thermal hysteresis (1 K) parallels the magnetic measurements, and it is a confirmation of the less cooperative character of the transition in this phen derivative. The thermal properties of **2** were also measured between 180 and 250 K in order to analyze the strange magnetic behavior observed in this temperature range (see the Supporting Information).[24] A featureless curve was

(24) Bhattacharjee, A.; Ksenofontov, V.; Sugiyarto, K. H.; Goodwin, H. A.; Gütlich, P. *Adv. Funct. Mater.* **2003**, *13*, 877.

obtained. The rehydrated compound **2r** exhibits a thermal behavior very similar to that of **2** (see the Supporting Information). The main difference is that dehydration takes place, as expected, at a slightly lower temperature (377 K).

The DSC measurement of **3** (Figure 17b, curve 1) affords three distinctive features located at 328, 338, and 343 K. The first two peaks correspond to desolvation of MeOH molecules bonded respectively to oxalate anions and water molecules. The third process should correspond to loss of water. Cooling the desolvated sample affords a very large and asymmetric feature that should be attributed to a small fraction of Fe^{2+} centers that undergo spin crossover. This result is in agreement with the magnetic data. The gradual and incomplete character of the transition precludes any analysis of the thermal parameters [enthalpy (ΔH) and entropy (ΔS) of the process, critical temperature, etc.] associated with it.[25] These parameters are listed in the Supporting Information for the different salts. They are in agreement with the assignments made in this chapter. Peaks assigned to spin transitions involve typical values of ΔH lying between 13.8 and 19.5 kJ·mol^{-1}. The same applies to ΔS, with values in the 38.3−58.8 J·K^{-1}·mol^{-1} range. Peaks assigned to dehydration processes involve higher energies (ΔH = 41.4−89.3 kJ·mol^{-1}). It is worth noting that rehydrated samples show smaller values of ΔH and ΔS, probably due to fatigue effects and faster desorption.

Solvent-Sensing Studies. The above results give compelling evidence of the role played by solvent molecules in the magnetic properties of the different complexes. It is clear that the magnetism of these simple salts can be very sensitive to other exchangeable guest solvents such as alcohols, which are able to form hydrogen bonds. In principle, a compound like **1**, showing an abrupt, hysteretic, and well-defined spin transition in its dehydrated phase could be used as a molecular probe in solvent sensing. Thus, **1** was dehydrated and resolvated with methanol. The process can be followed in a TGA apparatus. An increase of weight corresponding to one MeOH molecule per formula unit was observed. After the solvation process is finished, the sample is protected from the air and transferred to the SQUID. Magnetic measurements of this MeOH-solvated sample (**1s**) are markedly different compared to the rehydrated material. χT at low temperature (Figure 18) equals 4.8 emu·K·mol^{-1} and corresponds to 33% of Fe^{2+} cations in the HS state (note that the rehydrated material showed 100% of Fe^{2+} in the HS state). It remains practically constant upon heating to room temperature. At higher temperatures, an increase of χT is observed to give a maximum of around 330 K. This feature is reproducible, and it is likely due to the presence of traces of humidity in the SQUID. At further heating, desolvation starts and the magnetic signal increases abruptly, indicating the spin change. The desolvated sample is then characterized by its intrinsic spin-crossover behavior. It is the same as that observed for the dehydrated material.

(25) ΔH and ΔS were calculated by integrating the $C_p = f(T)$ functions across the different peaks: $\Delta H = \int_{T_1}^{T_2} C_p \, dT$; $\Delta S = \int_{T_1}^{T_2} (C_p/T) \, dT$.

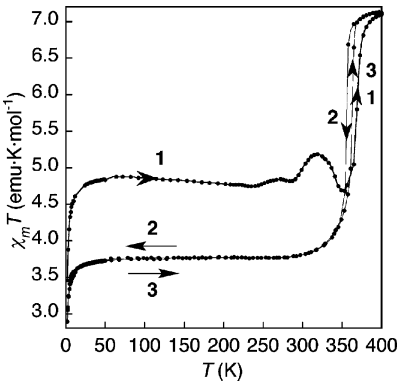

Figure 18. Temperature dependence of χT for **1s**. Curve 1: first heating. Curves 2 and 3: subsequent temperature cycles (cooling and heating, respectively).

Conclusion

Besides the previously mentioned reports concerning porous frameworks,[7−9] few other magnetostructural studies of desolvation−resolvation processes in spin-crossover simple salts have been undertaken.[26−29] These reports are limited to the characterization of the first LS → HS process accompanying dehydration and the observation of the intrinsic spin crossover of the anhydrous material at very low temperatures. The interest in these studies lies in the wide apparent hysteresis that results from the first heating−cooling cycle.[26−33] Further, in materials that do not rehydrate under ambient atmosphere, the spin crossover can be used as a "write-once" memory: after dehydration is completed, the material remains in its HS state provided it is not cooled at very low temperatures. It can thus be used as a thermal sensor, giving an optical or magnetic response only when the dehydration temperature is attained. Here, the materials can be used in combined temperature/humidity sensing: after heating to the temperature of control, a system such as **1** (initially having a HS fraction of 50%) can be found at room temperature in either HS or LS states, depending on the ambient humidity. In any case, further studies are needed for the development of a real application.

One of the important and novel aspects of the work is the analysis of the structural changes that occur after the irreversible dehydration−rehydration process. Important changes should be expected because the original materials are not porous and the water molecules are tightly bound to the ions via hydrogen bonding. The first point is the reduction of the cell parameters and, hence, of the number of

(26) Garcia, Y.; van Koningsbruggen, P. J.; Codjovi, E.; Lapouyade, R.; Kahn, O.; Rabardel, L. *J. Mater. Chem.* **1997**, *7*, 857−858.
(27) Garcia, Y.; van Koningsbruggen, P. J.; Lapouyade, R.; Fournès, L.; Rabardel, L.; Kahn, O.; Ksenofontov, V.; Levchenko, G.; Gütlich, P. *Chem. Mater.* **1998**, *10*, 2426−2433.
(28) Roubeau, O.; Haasnoot, J. G.; Codjovi, E.; Varret, F.; Reedijk, J. *Chem. Mater.* **2002**, *14*, 2559−2566.
(29) Sugiyarto, H.; Weitzner, K.; Craig, D. C.; Goodwin, H. A. *Aust. J. Chem.* **1997**, *50*, 869−874.
(30) Sorai, M.; Ensling, J.; Hasselbach, K. M.; Gütlich, P. *Chem. Phys.* **1977**, *20*, 197.
(31) Gütlich, P. *Struct. Bonding* **1981**, *44*, 83.
(32) Nakamoto, T.; Bhattacharjee, A.; Sorai, M. *Bull. Chem. Soc. Jpn.* **2004**, *77*, 921−932.
(33) Hayami, S.; Gu, Z.; Yoshiki, H.; Fujishima, A.; Sato, O. *J. Am. Chem. Soc.* **2001**, *123*, 11644−11650.

nonequivalent metal sites in the structure. The second aspect is the change of location of the water molecules of crystallization. Surprisingly, despite these changes, both **1** and **2** undergo dehydration and rehydration without loss of crystallinity. Indeed, this is the first report that gives a complete structural description of the changes in the spin state of the iron centers after rehydration.

The magnetic properties of **1** are very sensitive to the presence of different solvates. At room temperature, the anhydrous compound exhibits 100% of its Fe^{2+} centers in the LS configuration. After exposure to ambient humidity, the material undergoes a drastic change to 100% HS. This change is likely to be related to the substitution of one $[Cr(bpy)(ox)_2]^-$ anion by one water molecule in the second coordination sphere of the Fe^{2+} cations. However, solvation of this anhydrous sample with dry MeOH vapors affords a material with only 33% HS Fe^{2+} sites. The difference between the two solvation processes is probably due to a different extension of the hydrogen-bonded network in both salts. The differences in the magnetic properties of both solvated materials are enormous in comparison with the results obtained using some nanoporous frameworks.[7] They also occur at higher temperatures. Both aspects make these materials promising candidates for several applications, like solvent sensing or temperature control. Further studies are needed in order to probe the selectivity of the adsorption process for different solvents.

The $[Cr(phen)(ox)_2]^-$ anion affords two distinct salts (**2** and **3**) when combined with $[Fe(bpp)_2]^{2+}$. The structure and magnetic properties of **2** are very similar to those reported for **1**. The striking difference between the two salts concerns the products obtained after rehydration (**1r** and **2r**). Thus, whereas 100% of the Fe^{2+} cations in **1r** are HS at room temperature, most of the Fe^{2+} centers in **2r** are LS under the same conditions. This different behavior has been correlated to the distinct extent of hydration and location of the water molecules in the second coordination sphere of the iron cation. On the other hand, it is worth noting that the crystal structure of **3** contains four $[Cr(phen)(ox)_2]^-$ anions in the second coordination sphere of the iron cation. This situation seemed to guarantee a LS configuration for the iron center. However, the magnetic properties of **3** indicate a HS state in the whole temperature range. This might be due to a different arrangement of the hydrogen-bond acceptors in the vicinity of the amino groups, but it is also an indication of the impact of the packing of $[Fe(bpp)_2]^{2+}$ cations (aryl−aryl interactions) on the magnetic properties of the system. For a proper evaluation of the importance of these interactions, we propose a systematic study of the packing of cations in a family of $[Fe(bpp)_2]X_2$ salts. Optical and photomagnetic studies are also underway in order to analyze the optical response of the system and the interplay of the LIESST effect with the interesting sorption−desorption properties.

Acknowledgment. We thank José M. Martínez-Agudo for the magnetic measurements and for his help in the TGA/DSC experiments. This work was financially supported by the Spanish Ministerio de Educación y Ciencia (Grant MAT2004-3849) and Generalitat Valenciana.

Supporting Information Available: Figures S1 and S2 giving respectively $\chi T = f(T)$ and $M = f(H)$ plots for **4**, Figures S3 and S4 showing respectively the DSC measurements of **2** and **2r**, Table S1 listing the enthalpy and entropy data obtained from DSC measurements, and complete crystal structure details in CIF format. This material is available free of charge via the Internet at http://pubs.acs.org.

IC700910N